Article

General Method for Predicting Interface Bonding at Various Oxide–Metal Interfaces

Michiko Yoshitake [1,2]

1   National Institute for Materials Science (NIMS), Tsukuba 305-0047, Japan; yoshitake.michiko@nims.go.jp or materials.curation@gmail.com; Tel.: +81-298-5496
2   MatQ-lab, Chiba 271-0092, Japan

Abstract: Interface termination bonding between metal oxide and metals is discussed from the viewpoint of thermodynamics. The method of interface termination prediction proposed by the authors for Al_2O_3–metal and ZnO–metal interfaces is extended to a general interface between metal-oxide and metals. The extension of the prediction method to the interface between metal oxides and elemental semiconductors is also discussed. Information on interface bonding was extracted by carefully examining the experimental results and first-principles calculations in the references. The extracted information on interface bonding from references is compared with the results obtained via the proposed prediction method. It is demonstrated that interface termination bonding can be predicted by extending the method to oxide–metal interfaces in general, when there is no interface reaction such as the reduction of oxide, oxidation of metal, or mixed oxide formation. The method uses only basic quantities of pure elements and the formation enthalpy of oxides. Therefore, it can be applied to most of the metals (including elemental semiconductors) in the periodic table and metal oxides with one stable valence. The method is implemented as a software, "InterChemBond", and can be used free of charge.

Keywords: oxide–metal interface; interface chemistry; thermodynamic equilibrium; prediction software

1. Introduction

Interfaces between metals and oxides are practically very important for many applications. Strong interface bonds are necessary for solid-state bonding, thermal- or corrosion-resistant coatings, and production of composite materials. Band alignment at metal–oxide interfaces determines the performance of electric and optical devices including solar cells. Chemical reactions at metal–oxide interfaces govern the characteristics of catalysts, fuel cells, and batteries. Oxides can have a polar surface wherein the topmost surface is occupied by only oxygen atoms or the metal atoms constituting the oxide. Therefore, the interface between a metal and an oxide can be terminated either by oxygen or metal atoms. Since the interface-terminating species has a significant influence on bonding strength, wetting [1–5], and band alignment [6–13], it should be of great use in developing a method for the general prediction of interface chemical bonding (interface termination). So far, we have developed a general method to predict the interface-terminating species at Al_2O_3/metal interfaces [14,15] that uses only very basic parameters: molar volume, surface energy, vaporization enthalpy, and electron density at the boundary of the Wigner–Seitz cell for metals and Al (the metallic component of Al_2O_3), the chemical potential difference (work function difference) between metals and Al, and the formation enthalpy of metal oxides. The method has been successfully extended to ZnO/metal interfaces [16].

A system to give predicted results for the interface between various metals and Al_2O_3 or ZnO has been implemented as a web-based software, "InterChemBond", and anyone can use the software free of charge [17]. One example of a screenshot of the prediction with the software is shown in Figure 1. This screen shows the result of predicting the

interface bonding between Si-alloyed Ni and Al_2O_3, where the mother metal element (M_A, in this case Ni) and alloy metal element (M_B, in this case Si) are selected from the right side of the periodic table (with the radio button just below M_A and M_B on the left side, and which metal to be selected from the periodic table is chosen). Likewise, a type of oxide is selected from the bottom right of the periodic table. Here, one should choose the metal component of the oxide to be predicted. Then, the chemical formula of the oxides appears in a pull-down menu. For Al or Zn, only one oxide for each, Al_2O_3 or ZnO, respectively, appears. Then, by clicking the "Calculate" button on the left side, the predicted results are displayed below the "Calculation" button. In the figure, the interface bonding is predicted to be a Ni(Si) alloy, Si–O–Al–Al_2O_3 (the interface is terminated by oxygen atom), which agrees with experimental results [18].
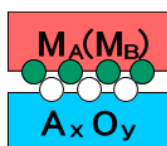
Figure 1. A screenshot of the prediction of interface bonding in Al_2O_3 and Ni (Si) alloy in the InterChemBond system.

In this article, the prediction method is extended to the interfaces with other oxides, and to the interfaces between elemental semiconductors (instead of metals) such as Si and Ge and various oxides. The predicted results are compared with carefully examined

experimental and theoretical results in the references. As described below, a thermodynamic equilibrium is considered only at the interface; the influence of the reduction of oxides or the oxidation of metals cause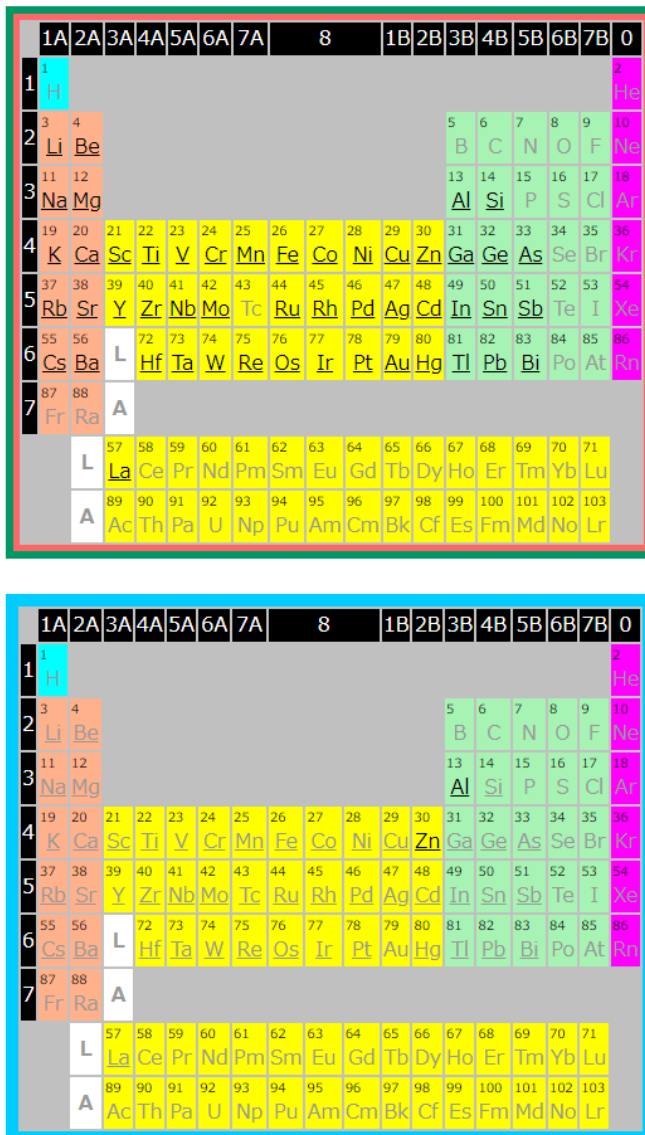d by the interface reaction is excluded. Due to this, interfaces with oxides having only one stable valence state are considered here. The condition without the presence of reactions such as oxidation or reduction can be clarified by the Ellingham diagram. If the user's condition (temperature and redox atmosphere at the interface) does not fall into the region of the reduction of oxide, or that of the oxidation of metal, the condition without the presence of reactions is maintained.

In the method, only polar interfaces in simple oxides composed of one metal component (A) and oxygen (O) will be considered. The interface between an electrode metal (M) and an oxide (AO) will be terminated either by (1) M-A-O-A—(called metal termination) or (2) M-O-A-O—(called oxygen termination). Thermodynamically, one of these terminations should be more stable than the other.

It should be noted that most of the contents of this manuscript have been uploaded to a preprint archive [19] and that the prediction software InterChemBond already works with the extended method described here.

2. Extension of the Prediction Method

2.1. Interface with Pure Metals including Elemental Semiconductors

For Al_2O_3/metal interfaces, we developed the prediction method [14,15]. The prediction method of ZnO/metal interfaces [16] was developed by extending the method used to predict Al_2O_3/metal interfaces. The prediction method considers terminating species within the frame of a chemical equilibrium. Because the formation enthalpy of most metal oxides ranges from that of Al_2O_3 to that of ZnO [20,21], it is considered reasonable to extend the prediction method for other oxides (AO) in general. Here, AO/metal interfaces in general are considered.

We assume a chemical equilibrium between the two terminations as shown in Equation (1).

$$\text{M-A-O—(metal termination)} + 1/2O_2 \rightleftharpoons \text{M-O-A-O—(oxygen termination)} \quad (1)$$
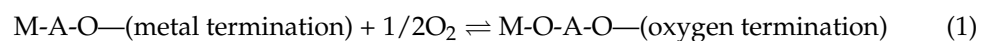
where the equilibrium constant, *K*, is represented by Equation (2).

$$K = \frac{a(\text{M} - \text{O} - \text{A} - \text{O}-)}{a(\text{M} - \text{A} - \text{O}-) \cdot \beta \cdot p(O_2)^{\frac{1}{2}}} \quad (2)$$

Here, $a(\text{M} - \text{O} - \text{A} - \text{O}-)a(\text{M} - \text{O} - \text{A} - \text{O}\cdots)$ is the activity of the oxygen-terminated interface, $a(\text{M} - \text{A} - \text{O}-)a(\text{M} - \text{A} - \text{O}\cdots)$ the activity of the metal-terminated one, $p(O_2)$ is the partial oxygen pressure, and β is a constant determined for each metal. The equilibrium occurs at the interface, where no oxygen gas exists, but the oxygen activity at the interface is proportional to the square root of the partial oxygen pressure [22]. This is the reason why $p(O_2)^{1/2}$ is in the numerator in Equation (2). The value of the equilibrium constant, *K*, can range from zero to infinity. When $K > 1$, the equilibrium in Equation (1) goes to the right side (oxygen termination), whereas the equilibrium goes to the left side when $K < 1$. *K* is related to the Gibbs energy, ΔG, of the reaction (1) through Equation (3):

$$K = \exp(-\Delta G / RT) \quad (3)$$

G = {chemical potential of (M-O-A-O—) at the standard condition}
  − {chemical potential of (M-A-O—) at the standard condition}   (4)
  − {half of oxygen chemical potential at the standard condition}

If the equilibrium in Equation (1) goes to the right side, the interface is oxygen-terminated, and vice versa. The equilibrium constant, *K*, which determines the direction of

the equilibrium, is determined by the Gibbs energy, which is a function of chemical potential for metal termination, that for oxygen termination and that for oxygen partial pressure.

We put the influence of oxygen partial pressure aside so that this term can be a constant in the range where oxides are not reduced, and so that the oxidation of the metals does not occur. Then, the chemical potential of metal termination is approximated by the M–A bonding energy and that of oxygen termination by the M–O bonding energy, as in the case of Al_2O_3 [14] and ZnO [16]. The M–A bonding energy is estimated either from the adsorption energy of A on M ($\equiv$X1), or by subtracting the adsorption energy of M on M from that of A on M ($\equiv$X2). The subtraction is used because the values of the adsorption energy include not only the influence of the chemical interaction between A and M but also that of the cohesion energy (upon adsorption, an adsorbed atom becomes a part of a solid). The adsorption energies were calculated using Miedema's formula [23] and by using the software [24] released by the author that calculates adsorption energies based on Miedema's formula. The M–O bonding energy is estimated either from the adsorption energy of oxygen on M (O on M, $\equiv$Y1), or by subtracting the dissociation energy of molecular oxygen from the adsorption energy of oxygen on M ($\equiv$Y2). The adsorption energy of oxygen on M is estimated from the oxide formation enthalpy via Equation (5), the details of which are described in ref. [14].

$$\text{adsorption energy of oxygen on M [kJ/mol-O]} = 0.719 \times \text{oxide formation enthalpy [kJ/mol-A]} + 230 \text{ [kJ/mol-O]} \qquad (5)$$

Using the two types of approximation for M–A and M–O bonding energies, two comparisons are used for predicting interface termination.

Approx-1: (A on M) vs. (O on M) (= X1 vs. Y1)
Approx-2: {(A on M) − (M on M)} vs. {(O on M) − 1/2(O_2 dissociation energy)} (= X2 vs. Y2),

where O_2 dissociation energy is 493.07 kJ/mol [25].

If (A on M) > (O on M)
and {(A on M) − (M on M)} > {(O on M) − 1/2(O_2 dissociation energy)},

the interface will be A-terminated (metal-terminated, having an M–A bond).

If (A on M) < (O on M)
and {(A on M) − (M on M)} < {(O on M) − 1/2(O_2 dissociation energy)},

then it will be O-terminated (oxygen-terminated, having an M–O bond).

If the comparison results with Approx-1 and Approx-2 are different, it means that the M–A and M–O bonding energies are close and can be influenced by conditions of the interface such as temperature and oxygen partial pressure. The flow of the prediction is summarized in Figure 2.

Now, we discuss the extension of the prediction method to elemental semiconductors (SC). Oxides of SCs are just the same as metal oxides: the values of the formation enthalpy of SiO_2 and GeO_2 are 910.7 and 580 (kJ/mol) [20], respectively. These values are between those of Al_2O_3 (1675.7 kJ/mol) and ZnO (350.5 kJ/mol). Regarding the adsorption energy of oxygen on Ge, the experimental values range from approximately 840 (kJ/mol) to 1050 (kJ/mol) [26], which are slightly larger than the value calculated (648.7 (kJ/mol)) using Equation (5). Because the values of (A on M_A) are more influenced by A rather than by M_A, and are smaller than the values of (O on M_A) in most combinations, using Equation (5) to estimate values of (O on MA) for SC is considered enough to predict interface termination. Furthermore, the adsorption energy of A on SC was reported to be simulated using the same equation as that for A on M [27], possibly because materials with SC–A bonding such as metal silicides and germanides are similar to intermetallic compounds. More accurately, 35 kJ/mol and 25 kJ/mol for Si and Ge, respectively, should be added to the values of the

enthalpy of mixing in alloys, which are used in the calculation of adsorption energy. This causes an adsorption energy increase by approximately 14 kJ/mol and 10 kJ/mol for Si and Ge, respectively. As seen in Section 4, these quantities are negligible when the values of A on M and O on M are compared. Due to these facts, it is considered reasonable to extend the prediction method to elemental semiconductors (instead of metals). For this reason, the addition of these values only for Si and Ge is not implemented in the software InterChemBond. This extension to elemental semiconductors also applies to interface prediction with the alloys described in the next section.
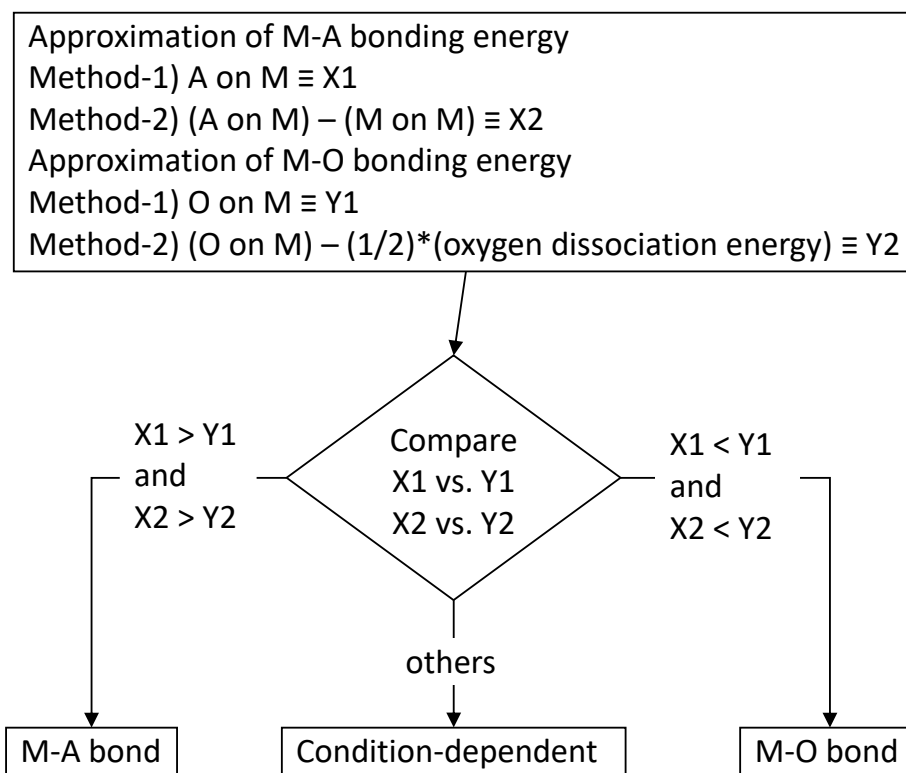

Figure 2. Procedure to predict interface termination between oxide (AO) and pure metal (M).

2.2. Interface with Alloys

Interface termination in oxide–alloy interfaces can be discussed by considering the effect of a second metal addition to the pure metal upon interface termination. Although, in general, metals (M) that form A termination at the metal oxide (AO) are very limited, a change from A termination to O termination can happen, as can a change from O termination to A termination, as explained for Al_2O_3 [15] and ZnO [16]. The chemical equilibrium at the interface with the alloy (the basic metal and additive metal are represented as M_A and M_B, respectively) is determined by the amount of energy stabilization due to interface bonding. Therefore, the adsorption energies of A on M_A ($\equiv$X1), O on M_A ($\equiv$Y1), A on M_B ($\equiv$XX1), and O on M_B ($\equiv$YY1) should be compared as shown in Figure 3. Here, only the approximation, Approx-1, used in the interface with pure metals is used to simplify the prediction method.

Just like the comparison between X1 and Y1 in Section 2.1 for judging whether the M–A bond or M–O bond is more stable, we should compare values among X1, Y1, XX1, and YY1. If XX1 is the largest among the four, this means the adsorption energy of A on M_B is the most stable, resulting in an A–M_B bond at the interface.
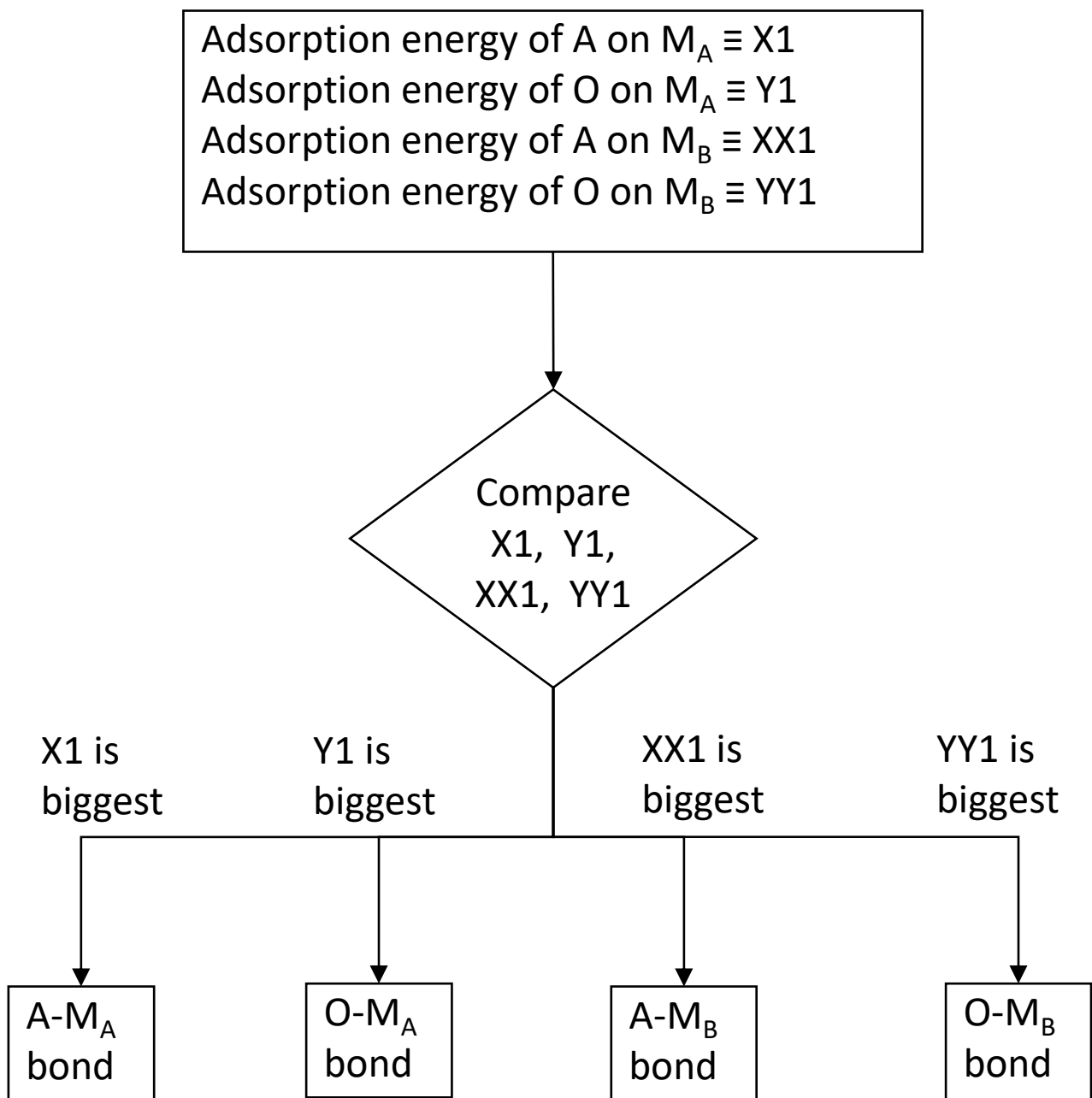
Figure 3. Procedure to predict interface termination between oxide (AO) and alloy ($M_A + M_B$).

3. Interface Termination in References

To examine interface termination in references, oxides mostly with only one stable valence, MgO, SiO_2, Cr_2O_3, Ga_2O_3, Y_2O_3, ZrO_2, CdO, La_2O_3, and HfO_2, are considered. This is because oxides with multivalence react with metals forming oxides with lower valence, which is not included in the present prediction method. In the following, the interface terminations in references are explained for each oxide–metal combination, and a concise summary is given in Table 1.

Table 1. Summary of reported interface terminations between oxides and metals in references.

Oxide (AO)	Orientation of Oxide	Metal (M)	Interface Termination		
			Experiment	Theory	References
MgO	{111}	Cu	O		[28]
	{222}	Cu	O		[29]
	(1–11)	Cu	O		[30]
	(111), (100)	Cu		O	[31]
	{222}	Cu(Ag)	O		[32,33]
	(1–11)	Pd	O		[30]
	(001)	Pd		O	[34]
	{100}	Ag	O		[35]
	{100}	Ag		O	[36]
	(001)	Ag		O	[37]
	(100)	Co		O	[38]
	(100)	Fe		O	[38]
	(001)	Ni		O	[34]
	(001)	Pt		O	[34]
	(001)	W		O	[34]
SiO$_2$		Al	O		[39]
		Au	Si		[39]
Cr$_2$O$_3$	(0001)	Ni		O	[40]
	(0001)	Ni		O	[41]
Ga$_2$O$_3$		Cr	O		[42]
Y$_2$O$_3$		Ge	O		[43]
ZrO$_2$	(111)	Ni	O		[44]
		Ni	Zr		[45]
		Ni	Zr		[46]
	(001)	Ni		O	[47]
	(111)	Ni		O	[48]
	(100)	Ni		O, Zr	[49]
		Cu	O		[50]
		Cu	O		[51]
	(−111)	Cu		O	[52]
		Co	O		[51]
		Pd	Zr		[53]
		Au	Zr		[54]
	(001)	Fe		O	[47]
	(001)	Si		O	[55]
CdO	{222}	Ag	O		[56]
	(001)	Ag		O	[57]
	{222}	Ag(Au)	Au-seg		[33]
La$_2$O$_3$		Si	O		[58]
		Si	O		[59]
	(001)	Ge		O	[60]
HfO$_2$		Si	O, Hf		[61,62]
		Si	O, Hf (exp + calc)		[63]
		Si		O	[64]
		Si		O	[65]
		Pt	O, Hf (exp + calc)		[65]

<MgO>

The interface with Cu was studied through the internal oxidation of Cu (Mg) single-phase alloys with different Mg concentrations, where Mg was fully oxidized so that no Mg remained in the alloy after oxidation. O termination has been observed via atom probe field ion microscopy (APFIM) [28], electron energy loss spectroscopy (EELS) [29], and

high-resolution transmission electron microscopy (HRTEM) [30]. Theoretical calculations also showed O termination [31].

When a Cu alloy not only with Mg but also Ag (Cu + 2.5 at.% Mg + 0.8 at.% Ag) was fully internally oxidized, Ag segregation and O termination were revealed via APFIM, EELS and scanning transmission electron microscopy (STEM) [32,33]. From the APFIM data in ref. [26], an O–Ag interface is inferred.

For the interface with Pd, O termination was observed at the interface via HRTEM using the fully internally oxidized Pd–1.5 wt.% Mg alloy [30]. Theoretical calculations also suggest O termination [34].

The interface with Ag was reported to be O-terminated from HRTEM experiments [35] and from theoretical calculations [36,37].

For the interface with Co and Fe, O termination is expected from theoretical calculations [38]. O termination is also expected from theoretical calculations for Ni, Pt, and W [34].

<SiO_2>

The interface with Al and Au has been experimentally studied, and O termination for Al and Si termination for Au have been reported [39].

<Cr_2O_3>

Only theoretical calculations for the interface with Ni, which showed O termination, have been reported [40,41].

<Ga_2O_3>

At the interface with Cr, the formation of Cr_2O_3 has been observed via transmission electron microscopy (TEM) [42], which means O termination.

<Y_2O_3>

The interface with Ge has been studied using X-ray photoelectron spectroscopy (XPS) during the growth of Y_2O_3 on Ge under molecular beam epitaxy (MBE) and showed Ge–O–Y bonding [43], which means O termination.

<ZrO_2>

Regarding the interface with Ni, a study on Ni film deposition on yttria-stabilized zirconia (111) using EELS revealed O termination at the Ni–ZrO_2 interface [44], while Zr termination was reported for the interface formed by the reduction of NiO–ZrO_2 from TEM and EELS observations [41] and for Ni–ZrO_2 composite plating, where the reduction of Zr4+ was observed by XPS [46]. In theoretical calculations, O termination has been reported to be energetically favorable both for ZrO_2 (001) [47] and ZrO_2 (111) [48]. In ref. [49], the oxygen partial pressure dependence of the stability of different terminations for different crystal orientations was discussed.

As for the interface with Cu, O termination was observed from an extended X-ray absorption fine structure (EXAFS) [50] and was suggested due to the existence of Cu ions at the interface observed via XPS [51]. With density functional theory (DFT) calculations, an optimized structure was reported to indicate O termination [52].

O termination is suggestive of an interface with Co from the existence of Co ions at the interface observed via XPS [51].

At the interface with Pd, Zr termination has been suggested from XPS measurements for ZrO_2 film on Pd (110) [53].

Zr termination has been reported at the interface with Au in nanocomposites from XPS measurements [54].

For the interface with Fe, O termination is suggestive for the ideal interface of ZrO (001) by DFT calculations from the work of adhesion [47].

The oxygen partial pressure dependence of the interface formation energy for ZrO (001)/Si interface has been calculated by the DFT method, and O termination is suggested to be stable for ordinary conditions [55].

<CdO>

The interface with Ag was observed to be O-terminated with CdO {222} by APFIM [56]. Theoretical calculations of the interface between Ag and CdO (001) reported O termination (involving interfacial hybridization of electrons between the Ag and O atoms) [57].

For the interface with Ag (Au) alloy, Au segregation at the interface was observed and the APFIM profile is suggestive of Cd termination [33].

<La_2O_3>

Interface with Si was experimentally studied by depositing La_2O_3 film on Si (100) and O termination (La–O–Si bonding at the interface) was observed via XPS [58]. Another study on La_2O_3 film deposition on Si (100) with XPS revealed the formation of La–silicate [59], which indicates O termination.

As for the interface with Ge, the interface stability of Ge (111) / La_2O_3 (001) was studied via DFT calculations, and O termination was determined to be more stable [60].

<HfO_2>

Interfaces with Si were studied by modeling the electric measurement (C–V characteristics) of the MOS structure, where Fermi-level pinning was suggested to occur due to Si–Hf bonds at the interface [61]. From the comparison between the modeling and the experiments, 20% of Si–O–Hf and 80% of Si–Hf bonds were indicated [62]. Another study suggested that there is a range of different interface configurations with mixed Hf–O and Hf–Si bonding [63]. Ref. [55] showed that the standard interface is fully O-terminated. First-principles thermodynamics calculations reported that the interface is silica-like, which indicates O termination [64].

For the interface with Pt, oxygen partial pressure dependence on interface termination was studied via first-principles thermodynamics calculations. The study showed that both O termination and Hf termination are possible depending on temperatures and pressures [64].

4. Comparison with Predicted Results

For each combination of an oxide and a metal described in Section 3, calculated values of X1, X2, Y1, Y2, XX1, and YY1, as well as the interface termination predictions according to the flowcharts in Figures 1 and 2, are demonstrated in Table 2. In the table, the values of the formation enthalpy of oxides, both for per oxide mole (usually in the database) and for per mol-metal in the oxide (mol-A), as well as the interface termination results from references explained in Section 3, are also listed. When more than one result either for experiments or theoretical calculations is reported, results are shown in the same column separated by "," for the same reference, and by ";" for a different reference in the table. There are some combinations at the interface not with a metal but with an elemental semiconductor such as Si and Ge. Interfaces of Si or Ge with Y_2O_3, ZrO_2, La_2O_3, and HfO_2 are regarded as model interfaces in the high-k oxide gate stack.

In Table 2, there is a clear disagreement between the prediction and the results from references only for Co/ZrO_2 and Cu/ZrO_2 among the 26 metal–oxide combinations (the disagreement is less than 8%). Concerning the interface with ZrO_2, most interfaces are predicted to show Zr termination due to the large values of X1 (the adsorption energy of Zr on metals). These large values come from large values of the mixing enthalpy of Zr in metals in Miedema's formula [23]. As seen in Table 2 of ref. [65], the enthalpy of alloy formation (=mixing enthalpy) calculated from Miedema's formula tends to be much larger (sometimes twice or three times larger) than the experimentally obtained values for Zr. If we take this into account, X1 values for ZrO_2 would be approximately 200 kJ smaller. Then, the prediction for both interfaces, Co/ZrO_2 and Cu/ZrO_2, becomes O termination, which agrees with the results in references. It is considered that the disagreement for the interface with ZrO_2 is due to the poor estimation of the mixing enthalpy of Zr using Miedema's formula.

Table 2. Calculated values of the adsorption energies of the metal component of an oxide, A, on metal M_A (A on M_A), that of oxygen on M_A (O on M_A), the subtracted values of {(A on M_A) − (M_A on M_A)} and {(O on M_A) − 1/2(O_2 dissociation energy)}, the adsorption energy of A on metal M_B (A on M_B), and that of oxygen on M_B (O on M_B). Values of oxide formation enthalpy for per oxide mole (usually in the database) and for per mol-metal (mol-M) are also listed. The values of the formation enthalpy of oxides are taken from ref. [20,21], where the value from ref. [21] is in italics in the table. The predicted results for each combination using these values are shown together with experimental and theoretical results from references.

Oxide AO	Metal-A M_A	Metal-B M_B	Formation Enthalpy of Oxide [kJ/mol]	Formation Enthalpy of Oxide [kJ/mol-A]	A on M_A X1	O on M_A Y1	A on M_A − M_A on M_A X2	O on M_A − 493.07/2 Y2	A on M_B XX1	O on M_B YY1	Prediction	Experiment	Theory
MgO	Cu		601.6	601.6	223	346.47	−42	99.935	-	-	O	O	O
	Cu	Ag			223	346.47	−42	99.935	160	242.69	O-Cu	O	
	Pd				324	295.06	41	48.525	-	-	Mg, O	O	O
	Ag				160	242.69	−62	−3.845	-	-	O	O	O
	Co				291	446.36	−44	199.825	-	-	O		O
	Fe				257	528.65	−59	282.115	-	-	O		O
	Ni				295	409	−45	162.465	-	-	O		O
	Pt				376	329.31	−72	82.775	-	-	Mg, O		O
	W				307	836.67	−388	590.135	-	-	O		O
SiO_2	Al		910.7	910.7	359	833.06	89	586.525	-	-	O	O	O
	Au				395	<0	102	<0	-	-	Si	Si	
Cr_2O_3	Ni		1139.7	569.85	313	409	−27	162.465	-	-	O		O; O
Ga_2O_3	Cr		1089.1	544.55	363	641.44	136	394.905	-	-	O	Ga_2O_3	
Y_2O_3	Ge		1905.3	952.65	389	648.7	92	402.165	-	-	O	Y_2O_3	
ZrO_2	Si		*1094.324*	*1094.324*	476	885.15	117	638.615			O		O
	Fe				588	528.65	272	282.115	-	-	Zr, O		O
	Co				622	446.36	287	199.825	-	-	Zr	O	
	Ni				629	409	289	162.465	-	-	Zr	O; Zr	Zr, O; O
	Cu				529	346.47	264	99.935	-	-	Zr	O	O
	Pd				660	295.06	377	48.525	-	-	Zr	Zr	
	Au				566	<0	273	<0–493.07/2			Zr	Zr	
CdO	Ag		258.4	258.4	112	242.69	−110	−3.845	-	-	O	O	O
	Ag	Au			112	242.69	−110	−3.845	159	<0	Cd-Ag	Au-seg	
La_2O_3	Ge		1793.7	896.85	435	648.7	138	402.165	-	-	O		O
	Si				459	885.15	100	638.615	-	-	O	O; O	
HfO_2	Si		1144.7	1144.7	444	885.15	85	638.615	-	-	O	O, Hf	O
	Si				444	885.15	85	638.615	-	-	O	Hf, O	
	Pt				671	329.31	223	82.775			O	Hf, O	

Except for Zr, the predictions are not sensitive to variations in input parameters. For example, for a MgO–Cu system, a 10% variation in molar volume causes less than a 3% variation in adsorption energy, and a variation of 10% in electron density results in approximately 10% variation in adsorption energy. The input parameters used are very basic and are not expected to vary much, such as 10%. Even if there are large variations such as 10% in input parameters, the predictions are not sensitive to variations in input parameters, because the energy differences (X1 vs. Y1; X2 vs. Y2) are more than 100 kJ/mol, and correspond to nearly 50% of the adsorption energy.

Regarding the interface with alloys, only two combinations were reported [28,29]. However, the main conclusion of the reports was solute segregation at the metal–oxide interface, and not much attention was paid to interface termination. Therefore, it is difficult to determine which type of interface bonding was realized in the experiments.

5. Conclusions

A method to predict the presence of an interface-terminating species at oxide–metal interfaces under thermodynamic equilibrium is proposed as an extension of our previous method for Al_2O_3–metal and ZnO–metal interfaces. This method is based on thermodynamics and uses only basic parameters of metals and oxides. The predicted results are compared with those of both experimental and theoretical studies on interface-terminating species at oxide–metal interfaces, which were carefully reviewed. Interfaces with oxides mostly having only one metal valence, MgO, SiO_2, Cr_2O_3, Ga_2O_3, Y_2O_3, ZrO_2, CdO, La_2O_3, and HfO_2, are discussed.

The procedure for interface prediction using the formula for pure metal (or elemental semiconductor), M, is briefly summarized as follows. First, calculate the values of the adsorption energies of metal component of the oxide, A, on metal M (A on M), that of M on M (M on M), and that of oxygen on M (O on M). Second, determine the signs of the expressions [(A on M) − (O on M)] (Approx-1) and [{(A on M) − (M on M)} − (O on M) − (493.07 kJ/mol)/2}] (Approx-2), where 493.07 kJ/mol is the dissociation energy of O_2. The interface will be A-terminated if the signs of the two expressions are positive and will be O-terminated if they are negative. If the sign of the two expressions is different, the interface termination could be condition-dependent.

For alloys composed of two metals, M_A and M_B, the procedure for predicting the interface between oxides and alloys using the formula is as follows. Here, we omit the corresponding procedure of Approx-2 used in the case of pure metal to simplify the formula. First, calculate the values of the adsorption energies of the metal component of the oxide, A, on metal M_A (A on M_A) and on metal M_B (A on M_B), and that of oxygen on M_A (O on M_A) and on M_B (O on M_B). Second, compare these values and find which is the largest. When (A on M_A) is the largest, the interface is predicted to be A-terminated with an A–M_A bond. If (O on M_A) is the largest, O termination with an O–M_A bond is predicted. A termination with an A–M_B bond is predicted when (A on M_B) is the largest, while O termination with an O–M_B bond is predicted if (O on M_B) is the largest.

In principle, interface termination depends on the temperature and the partial pressure of oxygen. Therefore, these influences should be taken into account for more accurate and precise prediction. Furthermore, the Gibbs energy of interface termination, which should depend on crystal orientations of the metal and oxide in contact, is approximated with the very simple and brief procedure in this method. However, it has been demonstrated that the predictions of interface termination mostly agree with the reported experimental results and explain the results of theoretical calculations. Hence, the prediction method should be useful for screening materials for developing interfaces since the method is based on thermodynamics, and uses only basic parameters of metals and oxides, being applicable to various oxide–metal combinations. The prediction procedure is implemented as a web-based software in InterChemBond [17], where users can obtain predicted results by choosing a metal and an oxide from the periodic table.

In this report, we exclude the formation of the interface with reactions. It is possible that the reduction of oxides from the most stable oxide we treated in this paper to a less stable one may occur, where either the slight oxidation of the contacting metal at the interface or the dissolution of oxygen atoms into the contacting metal might happen. The oxidation of the contacting metal at the interface forms a mixed oxide, the oxide consisting both the metal component of the original oxide (A) and the contacting metal, M. The interface termination prediction that takes such an interface reaction into account will be discussed in a separate paper in the near future.

References

1. Alber, U.; Mullejans, H.; Ruhle, M. Wetting of copper on α-Al$_2$O$_3$ surfaces depending on the orientation and oxygen partial pressure. *Micron* **1999**, *30*, 101–108. [CrossRef]
2. Merlin, V.; Eustathopoulos, M. Wetting and adhesion of Ni-Al alloys on α-Al$_2$O$_3$ single crystals. *J. Mater. Sci.* **1995**, *30*, 3619–3624. [CrossRef]
3. Chantain, D.; Chabert, F.; Ghetta, V.; Fouletier, J. New Experimental Setup for Wettability Characterization under Monitored Oxygen Activity: II, Wettability of Sapphire by Silver-Oxygen Melts. *J. Am. Ceram. Soc.* **1994**, *77*, 197–201. [CrossRef]
4. Shi, S.; Tanaka, S.; Kohyama, M. First-principles study of the tensile strength and failure of α-Al$_2$O$_3$/Ni(111) interfaces. *Phys. Rev.* **2007**, *B76*, 075431. [CrossRef]
5. Shi, S.; Tanaka, S.; Kohyama, M. First-Principles Investigation of the Atomic and Electronic Structures of α-Al$_2$O$_3$/Ni(111) Interfaces. *J. Am. Ceram. Soc.* **2007**, *90*, 2429–2440. [CrossRef]
6. Shi, S.; Tanaka, S.; Kohyama, M. Influence of interface structure on Schottky barrier heights of α-Al$_2$O$_3$ (0001)/Ni (111) interfaces: A first-principles study. *Mater. Trans.* **2006**, *47*, 2696–2700. [CrossRef]
7. Shiraishi, K.; Nakayama, T.; Nakaoka, T.; Ohta, A.; Miyazaki, S. Theory of Metal/Dielectric Interfaces-Breakdown of Schottky Barrier Limits. *ECS Trans.* **2008**, *13*, 21–27. [CrossRef]
8. Nagata, T.; Ahmet, P.; Yoo, Y.Z.; Yamada, K.; Tsutsui, K.; Wada, Y.; Chikyow, T. Schottky metal library for ZNO-based UV photodiode fabricated by the combinatorial ion beam-assisted deposition. *Appl. Surf. Sci.* **2006**, *252*, 2503–2506. [CrossRef]
9. Asthagiri, A.; Niederberger, C.; Francis, A.J.; Porter, L.M.; Salvador, P.A.; Sholl, D.S. Thin Pt films on the polar SrTiO$_3$ (111) surface: An experimental and theoretical study. *Surf. Sci.* **2003**, *537*, 134–152. [CrossRef]
10. Yoshitake, M.; Nemsak, S.; Skala, T.; Tsud, N.; Kim, T.; Matolin, V.; Prince, K.C. Modification of terminating species and band alignment at the interface between alumina films and metal single crystals. *Surf. Sci.* **2010**, *604*, 2150–2156. [CrossRef]
11. Ip, K.; Thaler, G.T.; Yang, H.; Han, S.Y.; Li, Y.; Norton, D.P.; Pearton, S.J.; Jang, S.; Ren, F. Contacts to zno. *J. Cryst. Growth* **2006**, *287*, 149–156. [CrossRef]
12. Young, S.J.; Ji, L.W.; Chang, S.J.; Su, Y.K. ZnO metal–semiconductor–metal ultraviolet sensors with various contact electrodes. *J. Cryst. Growth* **2006**, *293*, 43–47. [CrossRef]
13. Lin, T.K.; Chang, S.J.; Su, Y.K.; Huang, B.R.; Fujita, M.; Horikoshi, Y. ZnO MSM photodetectors with Ru contact electrodes. *J. Cryst. Growth* **2005**, *281*, 513–517. [CrossRef]
14. Yoshitake, M.; Yagyu, S.; Chikyow, T. Novel method for the prediction of an interface bonding species at alumina/metal interfaces. *J. Vac. Sci. Technol.* **2014**, *A32*, 021102. [CrossRef]
15. Yoshitake, M.; Yagyu, S.; Chikyow, T. A numerical formula for general prediction of interface bonding between alumina and aluminum-containing alloys. *Int. J. Met.* **2014**, *2014*, 120840. [CrossRef]
16. Yoshitake, M. General method for predicting ZnO–metal interface termination: Extension of the method for Al$_2$O$_3$–metal systems. *J. Vac. Sci. Technol.* **2021**, *A39*, 063217. [CrossRef]
17. InterChemBond. Available online: https://interchembond.nims.go.jp (accessed on 23 October 2022).
18. Yoshitake, M.; Nemšák, S.; Skála, T.; Tsud, N.; Matolín, V.; Prince, K.C. The influence of Si in Ni on the interface modification and the band alignment between Ni and alumina. *Appl. Surf. Sci.* **2018**, *442*, 164–169. [CrossRef]
19. Yoshitake, M. General method for predicting interface bonding at various oxide-metal interfaces. *Jxiv* **2022**. [CrossRef]
20. Lide, D.R. (Ed.) *CRC Handbook of Chemistry and Physics*, 74th ed.; CRC: Boca Raton, FL, USA, 1993–1994.
21. Brewer, L. The thermodynamic properties of the oxides and their vaporization processes. *Chem. Rev.* **1953**, *52*, 1–75. [CrossRef]
22. Muolo, M.L.; Valenza, F.; Passerone, A.; Passerone, D. Oxygen influence on ceramics wettability by liquid metals: Ag/α-Al$_2$O$_3$—Experiments and modelling. *Mater. Sci. Enginnering* **2008**, *A495*, 153–158. [CrossRef]

23. Miedema, A.R.; Dorleijn, J.W.F. Quantitative predictions of the heat of adsorption of metals on metallic substrates. *Surf. Sci.* **1980**, *95*, 447–464. [CrossRef]

24. SurfSeg. Available online: https://surfseg.nims.go.jp (accessed on 3 April 2024).

25. Brix, P.; Herzberg, G. Fine structure of the Schumann-Runge bands near the convergence limit and the dissociation energy of the oxygen molecule. *Can. J. Phys.* **1954**, *32*, 110–135. [CrossRef]

26. Green, M.; Kafalas, J.A.; Robinson, P.H. The interaction of oxygen with clean germanium surfaces. In *Semiconductor Surface Physics, Proceedings of the Conference on the Physics of Semiconductor Surface, Philadelphia, PA, USA, 4–6 June 1956*; Kingston, R.H., Ed.; University of Pennsylvania Press: Philadelphia, PA, USA, 1957; pp. 349–361.

27. Miedema, A.R.; Chatel, P.F.; Boer, F.R. Cohesion in alloys–fundamentals of a semi-empirical model. *Physica* **1980**, *100B*, 1–28. [CrossRef]

28. Jang, H.; Seidman, D.N.; Merkle, K.L. The chemical composition of a metal/ceramic interface on an atomic scale: The Cu/MgO {111} interface. *Interface Sci.* **1993**, *1*, 61–75. [CrossRef]

29. Muller, D.A.; Shashkov, D.A.; Benedek, R.; Yang, L.H.; Silcox, J.; Seidman, D.N. Atomic Scale Observations of Metal-Induced Gap States at {222} MgO/Cu Interfaces. *Phys. Rev. Lett.* **1998**, *80*, 4741–4744. [CrossRef]

30. Chen, F.R.; Chiou, S.K.; Chang, L.; Hong, C.S. High-resolution electron microscopy of Cu/MgO and Pd/MgO interfaces. *Ultramicroscopy* **1994**, *54*, 179–191. [CrossRef]

31. Benedek, R.; Minkoff, M.; Yang, L.H. Adhesive energy and charge transfer for MgO/Cu heterophase interfaces. *Phys. Rev.* **1996**, *B54*, 7697–7700. [CrossRef]

32. Shashkov, D.A.; Chisholm, M.F.; Seidman, D.N. Atomic-scale structure and chemistry of ceramic/metal interfaces—I. Atomic structure of {222} MgO/Cu (Ag) interfaces. *Acta Mater.* **1999**, *47*, 3939–3951. [CrossRef]

33. Shashkov, D.A.; Chisholm, M.F.; Seidman, D.N. Atomic-scale structure and chemistry of ceramic/metal interfaces—II. Solute segregation at MgO/Cu (Ag) and CdO/Ag (Au) interfaces. *Acta Mater.* **1999**, *47*, 3953–3963. [CrossRef]

34. Yudanov, I.; Pacchioni, G.; Neyman, K.; Rosch, N. Systematic density functional study of the adsorption of transition metal atoms on the MgO (001) surface. *J. Phys. Chem.* **1997**, *B101*, 2786–2792. [CrossRef]

35. Trampert, A.; Ernst, F.; Flynn, C.P.; Fischmeister, H.F.; Ruhle, M. High resolution transmission electron microscopy studies of the Ag/MgO interface. *Acta Metall. Mater.* **1992**, *40*, S227–S236. [CrossRef]

36. Schonberger, U.; Anderson, O.K.; Methfessel, M. Bonding at metal-ceramic interfaces; ab initio density-functional calculations for Ti and Ag on MgO. *Acta Metall. Mater.* **1992**, *40*, S1–S10. [CrossRef]

37. Li, C.; Wu, R.; Freeman, A.J.; Fu, C.L. Energetics, bonding mechanism, and electronic structure of metal-ceramic interfaces: Ag/MgO (001). *Phys. Rev.* **1993**, *B48*, 8317–8322. [CrossRef] [PubMed]

38. Yang, H.X.; Chshiev, M.; Dieny, B.; Lee, J.H.; Manchon, A.; Shin, K.H. First-principles investigation of the very large perpendicular magnetic anisotropy at Fe∣MgO and Co∣MgO interfaces. *Phys. Rev.* **2011**, *B84*, 054401. [CrossRef]

39. Bauer, R.S.; Bachrach, R.Z.; Brillson, L.J. Au and Al interface reactions with SiO_2. *Appl. Phys. Lett.* **1980**, *37*, 1006–1008. [CrossRef]

40. Hui, L.; Yuping, L.; Caili, Z.; Nan, D.; Aidong, L.; Hongfei, L.; Hongbiao, D.; Peide, H. Effects of aluminum diffusion on the adhesive behavior of the Ni (111)/Cr_2O_3 (0001) interface: First principle study. *Comput. Mater. Sci.* **2013**, *78*, 116–122. [CrossRef]

41. Hui, L.; Yuping, L.; Caili, Z.; Nan, D.; Hongfei, L.; Hongbiao, D.; Peide, H. The tensile properties and fracture of the Ni/Cr_2O_3 interface: First principles simulation. *Comput. Mater. Sci.* **2014**, *82*, 367–371. [CrossRef]

42. Aller, H.T.; Yu, X.; Wise, A.; Howell, R.S.; Gellman, A.J.; McGaughey, A.J.H.; Malen, J.A. Chemical Reactions Impede Thermal Transport Across Metal/β-Ga_2O_3 Interfaces. *Nano Lett.* **2019**, *19*, 8533–8538. [CrossRef]

43. Chu, L.K.; Lee, W.C.; Huang, M.L.; Chang, Y.H.; Tung, L.T.; Chang, C.C.; Lee, Y.J.; Kwo, J.; Hong, M. Metal-oxide-semiconductor devices with molecular beam epitaxy-grown Y_2O_3 on Ge. *J. Cryst. Growth* **2009**, *311*, 2195–2198. [CrossRef]

44. Sasaki, T.; Matsunaga, K.; Ohta, H.; Hosono, H.; Yamamoto, T.; Ikuhara, Y. Atomic and electronic structures of Ni/YSZ (111) interface. *Mater. Trans.* **2004**, *JIM 45*, 2137–2143. [CrossRef]

45. Wang, W.; Guo, H.T.; Gao, J.P.; Dong, X.H.; Qin, Q.X. XPS, UPS and ESR studies on the interfacial interaction in Ni-ZrO_2 composite plating. *J. Mater. Sci.* **2000**, *35*, 1495–1499. [CrossRef]

46. Dickey, E.C.; Dravid, V.P.; Nellist, P.D.; Wallis, D.J.; Pennycook, S.J.; Revcolevschi, A. Structure and bonding at Ni–ZrO_2 (cubic) interfaces formed by the reduction of a NiO–ZrO_2 (cubic) composite. *Microsc. Microanal.* **1997**, *3*, 443–450. [CrossRef]

47. Eremeev, S.V.; Schmauder, S.; Hocker, S.; Kulkova, S.E. Ab-initio investigation of Ni (Fe)/ZrO_2 (001) and Ni–Fe/ZrO_2 (001) interfaces. *Surf. Sci.* **2009**, *603*, 2218–2225. [CrossRef]

48. Christensen, A.; Carter, E.A. Adhesion of ultrathin ZrO_2 (111) films on Ni(111) from first principles. *J. Chem. Phys.* **2001**, *114*, 5816–5831. [CrossRef]

49. Munoz, M.C.; Gallego, S.; Beltran, J.I.; Cerda, J. Adhesion at metal–ZrO_2 interfaces. *Surf. Sci. Rep.* **2006**, *61*, 303–344. [CrossRef]

50. Liu, S.-H.; Wang, H.P.; Wang, H.-C.; Yang, Y.W. In situ EXAFS studies of copper on ZrO_2 during catalytic hydrogenation of CO_2. *Electron. Spectrosc. Relat. Phenom.* **2005**, *144–147*, 373–376. [CrossRef]

51. Ikonomov, J.; Stoychev, D.; Marinova, T. XPS and SEM characterization of electrodeposited transition metals on zirconia. *Appl. Surf. Sci.* **2000**, *161*, 94–104. [CrossRef]

52. Tang, Q.-L.; Hong, Q.-J.; Liu, Z.-P. CO_2 fixation into methanol at Cu/ZrO_2 interface from first principles kinetic Monte Carlo. *J. Catal.* **2009**, *263*, 114–122. [CrossRef]

53. Guo, Q.; Joyner, R.W. An X-ray photoelectron spectroscopy study of the stability of ZrO_2 films on Pd (110). *Appl. Surf. Sci.* **1999**, *144–145*, 375–379. [CrossRef]

54. Zhang, X.; Wang, H.; Xu, B.-Q. Remarkable Nanosize Effect of Zirconia in Au/ZrO_2 Catalyst for CO Oxidation. *J. Phys. Chem.* **2005**, *B109*, 9678–9683. [CrossRef]

55. Peacock, P.W.; Xiong, K.; Tse, K.; Robertson, J. Bonding and interface states of $Si:HfO_2$ and $Si:ZrO_2$ interfaces. *Phys. Rev.* **2006**, *B73*, 075328. [CrossRef]

56. Chan, D.K.; Jang, H.; Seidman, D.N.; Merkle, K.L. Initial results on the Ag [vert bar] CdO [222] interface: Atomic scale interfacial chemistry and sequencing of ordered cadmium/oxygen planes. *Scri. Metall. Mater.* **1993**, *29*, 1119–1124. [CrossRef]

57. Rao, F.; Wu, R.; Freeman, A.J. Structure and bonding at metal-ceramic interfaces: Ag/CdO (001). *Phys. Rev.* **1995**, *B51*, 10052–10056. [CrossRef]

58. Capodieci, V.; Wiest, F.; Sulima, T.; Schulze, J.; Eisele, I. Examination and evaluation of La_2O_3 as gate dielectric for sub-100 nm CMOS and DRAM technology. *Microelectron. Reliab.* **2005**, *45*, 937–940. [CrossRef]

59. Ablat, A.; Mamat, M.; Ghupur, Y.; Aimidula, A.; Wu, R.; Baqi, M.A.; Gholam, T.; Wang, J.; Qian, H.; Wu, R.; et al. Electronic structure of La_2O_3/Si interface by in situ photoemission spectroscopy. *Mater. Lett.* **2017**, *191*, 97–100. [CrossRef]

60. Liu, K.; Ko, E.; Hwang, C.S.; Choi, J.-H. A first-principles study of the structural and electronic properties of the epitaxial Ge $(111)/La_2O_3$ (001) heterostructure. *J. Phys. D Appl. Phys.* **2019**, *52*, 365101. [CrossRef]

61. Hobbs, C.C. Hegde. Fermi-Level Pinning at the Polysilicon/Metal Oxide Interface: Part I. *IEEE Trans. Electron. Devices* **2004**, *51*, 971–977. [CrossRef]

62. Hobbs, C.C.; Fonseca, L.R.C.; Knizhnik, A.; Dhandapani, V.; Samavedam, S.B.; Taylor, W.J.; Grant, J.M.; Dip, L.G.; Triyoso, D.H.; Hegde, R.I.; et al. Fermi-level pinning at the polysilicon/metal-oxide interface-Part II. *IEEE Trans. Electron. Devices* **2004**, *51*, 978–984. [CrossRef]

63. Xiong, K.; Peacock, P.W.; Robertson, J. Fermi level pinning and Hf–Si bonds at HfO_2: Polycrystalline silicon gate electrode interfaces. *Appl. Phys. Lett.* **2005**, *86*, 012904. [CrossRef]

64. Zhu, H.; Tang, C.; Ramprasad, R. Phase equilibria at $Si-HfO_2$ and $Pt-HfO_2$ interfaces from first principles thermodynamics. *Phys. Rev.* **2010**, *B82*, 235413. [CrossRef]

65. Miedema, A.R.; Boom, R.; Boer, F.R. On the heat of formation of solid alloys. *J. Less-Common Met.* **1975**, *41*, 283–298. [CrossRef]